Modeling Offset-Dependent Reflectivity for Time-Lapse Monitoring of Water-Flood Production in Thin-Layered Reservoirs

Shelley J. Ellison

Thesis submitted to the Faculty of the Virginia Polytechnic Institute and State University in partial fulfillment of the requirements for the degree of

Master of Science
in
Geophysics

Dr. Matthias Imhof, Chair

Dr. Cahit Çoruh,

D. Alan Fuqua

Stephen C. Henry

July 10, 2001
Blacksburg, Virginia

Keywords: Geophysics, AVO, Reservoir Characterization

Modeling Offset-Dependent Reflectivity for Time-Lapse Monitoring of Water-Flood Production in Thin-Layered Reservoirs

Shelley J. Ellison

(ABSTRACT)

Seismic time-lapse monitoring of production is an important tool used to efficiently drain a hydrocarbon reservoir. Repeat seismic surveys may be used, because the seismic method is sensitive to the reservoir fluid. A prominent seismic attribute is the reflectivity (or amplitude) as a function of offset (AVO) which strongly depends on material properties, and hence, on the pore fluid. Repeat surveys, however, are very costly. To reduce the risks, the repeat survey is simulated on a computer for a number of different scenarios. Hence, the objectives of this study are to predict the seismic responses after five years of production of the reservoirs at the well locations, correlate the seismic attributes to fluid conditions in the reservoirs, assess the detectability of changes in AVO attributes due to changes in fluid conditions, and determine which attribute is more diagnostic of fluid changes.

Petrophysical models were generated for different pore fluids using well logs from a field in the Gulf of Mexico. Synthetic seismograms were then calculated using a layerstack scheme to study the effects of the reservoir fluids on AVO. Compared to idealized half-space models, it was found that the AVO responses are contaminated by

the overburden and the thinness of the reservoir. In order to remove transmission loss due to overburden effects, the synthetic AVO curves were scaled by normalizing an overburden-over-half-space model to an idealized analytical Zoeppritz model. In a second step, an offset-dependent overburden correction was applied using a low order polynomial, which was fitted to the amplitude ratios between the overburden/half-space model and the idealized model. Finally, a zero-offset tuning correction was applied.

The results of the AVO analyses showed that some errors were unresolved using the applied overburden and tuning corrections, and amplitudes at large offsets were possibly contaminated by multiples and converted waves. Since there is no shallower production or steam injection for this particular field, the repeat surveys should have the same overburden, tuning, multiple-related and converted wave contamination. It appears reasonable to assume that any changes in amplitude between the repeat surveys would be due to fluid saturation changes. Therefore, it was concluded that it is not necessary to attempt to remove the overburden and tuning effects.

Results from the AVO analyses of the uncorrected models showed that AVO attributes should be a useful tool to detect reservoir conditions during the production of the field. Generally, the water-flood changes the AVO by decreasing the intercept and increasing the gradient from the in-situ oil/gas cases. The relative changes in both intercept and gradient due to the water-flood are detectable assuming a 20% relative-change detection threshold, and gradient is more diagnostic because the relative change in gradient is very large compared to that for intercept.

RESEARCH CONTRIBUTIONS

The author wishes to acknowledge Texaco Inc. for the well logs, seismic data, software, and internships made available for thesis work, and to Mike Greene, Brian O'Neill, and the many people that have provided technical assistance, advice and support. GeoGraphix, Hampson-Russell and Rock Solid Images are appreciated for granting student licenses, software, and helpful technical support. The Department of Geological Sciences of Virginia Tech has also aided in this research project through the Texaco Geophysics Scholarship as well as by providing teaching and research assistantships.

AUTHOR'S ACKNOWLEDGEMENTS

I would like to thank Texaco Inc. for the well logs, seismic data, and software made available for thesis work. I am also grateful to Texaco for providing me with a scholarship, along with opportunities to learn and grow through summer internships. My deepest appreciation goes to my committee members, Dr. Matthias Imhof, Dr. Cahit Çoruh, Alan Fuqua, and Steve Henry for the many hours spent working with me, for their continued support, and for keeping me on the straight and narrow path. Special thanks go to several people at Texaco that have provided technical assistance and advice, especially Brian O'Neill and Mike Greene, who championed a multitude of problem-solving, long-distance telephone calls. At Virginia Tech, Eric Wonderley and Mark Lemon deserve many thanks for their diligence in maintaining computers/software, without which work is impossible. I will miss all of my fellow graduate students as well as the staff in the main office in the Department of Geological Sciences. With smiling faces and helping hands, they have assisted me in remaining a happy and productive member of the department. Among them, I wish to especially thank Connie Lowe for all of the times I entered her office overwhelmed and dejected, and left reassured and revitalized. A special thank you goes to my wonderful new husband and best friend, Pat Tyree, for putting up with the lonely summers when I was away, and the high stress level when I was home working on my thesis. Lastly, to my parents, Steve and Debbie Ellison, who still had faith in me when I said that I wanted to be a geophysicist when I grew up, thank you for the values you instilled in me, for your bottomless cup of pride, and for supporting me in the achievement of my every goal.

TABLE OF CONTENTS

INTRODUCTION

Recent experiments have shown that seismic time-lapse monitoring has the potential to become a very powerful tool for understanding reservoir behavior while maximizing long-term production. For example, the motivation of the project discussed here is to use time-lapse seismic data to monitor the behavior of some reservoirs for which the production is assisted by water injection. By tracking the movement of the waterfront through the field, one may observe how efficiently the reservoirs are drained, and detect the formation of disconnected pockets of hydrocarbons and bypassed reserves.

Costs of repeat surveys, however, are a major problem due to the stringent requirements on data acquisition and processing to ensure consistency between surveys (e.g., Ebrom et al, 1998). For any particular project, it is crucial to test the feasibility of monitoring as well as to determine the optimum times to perform follow-up surveys (e.g., Wang, 1997). In a time-lapse experiment, a base seismic survey of a reservoir is acquired prior to production. After some time has passed during production, at least one more seismic survey is acquired. If the acquisition and processing of the surveys are as similar as possible, and they have been equalized as well (e.g., Chiburis, 1987), it may be assumed that differences between the surveys are due to changes in the fluid conditions of the reservoir since there should not be any changes in the overburden or the lithology of the reservoir (Wang, 1997). An important caveat is that production from a shallower reservoir could change the overburden characteristics affecting the base and time-lapsed seismic surveys. For this study, production will be limited to three reservoirs within a several hundred-foot depth interval with no shallower production.

Seismic surveys are very expensive. Before expending large sums of capital, oil companies want to ascertain the expected changes in fluid conditions in the reservoir are seismically detectable before acquiring the repeat survey. Therefore, the purpose of this study is to simulate the time-lapse environment and predict the seismic response of the reservoir after five years of production. This is done, first, by using field well log data to create a petrophysical model, from which the synthetic seismic response is computed for the in-situ reservoir. To validate the petrophysical model, the synthetic seismic data must be compared to the field data. Then, using a fluid flow simulation model to predict the reservoir parameters (i.e., fluid saturations, pressure, etc.) after five years of production, a new petrophysical model is constructed, from which we calculate the seismic response of the producing reservoir. A number of seismic attributes can be built from the two data sets. Since the overburden or the reservoir lithology do not change, all differences in the data sets can be attributed to the reservoir fluids. Hence, the objectives of this study are threefold: (1) forward model the reservoirs at initial conditions and after five years to predict the seismic responses; (2) determine how seismic attributes, i.e., amplitude versus offsets (AVO), are affected by the different fluids; and (3) assess the sensitivity and usefulness of the different attributes in light of the differences in data acquisition, data processing, and data quality.

We found that relating absolute changes of attributes to reservoir changes is very difficult, as a number of ill-defined corrections would be needed. Relative changes of attributes, however, may be easier to evaluate.

AVO Attributes

An amplitude recorded on a seismic trace is due to energy partitioning of the incident P-wave into transmitted and reflected P- and S-waves at an interface separating two homogeneous, isotropic, elastic half-spaces given by velocities (V_{P1}, V_{P2}, V_{S1}, V_{S2}) and densities (ρ_1, $\rho_{2)}$ (e.g., Castagna, 1993). The ratios between the different phases depend on the angle of incidence of the incoming P-wave. Furthermore, these ratios are strongly dependent on the material properties of the half-spaces. While the reflections, transmissions, and conversions are completely described by the Zoeppritz (1919) equations, one often uses Shuey's approximation (1985) when dealing with experimentally measured amplitude versus offset (AVO) behavior. Shuey reduced the complex Zoeppritz equations to a single two-parameter approximation:

$$R_{pp}(\theta) \approx A + B\sin^2\theta, \qquad (1)$$

where θ is angle of incidence, A is the AVO intercept and B is the AVO gradient. A is approximately the normal incidence ($\theta = 0°$) reflection coefficient, and is due to the acoustic impedance contrast across the interface, where impedance is the product of P-wave velocity and density:

$$A = \frac{\rho_2 V_{P2} - \rho_1 V_{P1}}{\rho_2 V_{P2} + \rho_1 V_{P1}}. \qquad (2)$$

B is controlled by the change in Poisson's ratio across the interface, which is related to the change in shear strength. Poisson's ratio (σ) is defined as:

$$\sigma = \frac{\left(V_P^{\,2} - 2V_S^{\,2}\right)}{2\left(V_P^{\,2} - V_S^{\,2}\right)}. \qquad (3)$$

B is related to Poisson's ratio as suggested by Hilterman (1989) by the following equation:

$$B = \frac{\sigma_2 - \sigma_1}{(1-\sigma)^2}. \qquad (4).$$

In practice, one often picks the amplitude of a reflection as a function of offset. These amplitudes are mapped from the offset domain to the incident angle domain and plotted as reflectivity versus angle of incidence (Figure 1). The intercept A is approximately the amplitude R(0) at zero offset, and the gradient is determined by the shape of the dashed curve. For restricted angles of incidence, i.e. less than 30°, the curve becomes linear in $\sin^2\theta$ as shown in the diagram on the right, and the gradient may be taken as the slope of the line (Castagna, 1993).

In the discussion that follows, we investigate the AVO attributes of our models, quantify the changes in attributes from the in-situ to 5-year case, and determine whether these changes are seismically detectable.

Geologic Setting

The reservoirs of interest in this study (Figure 2) are three Middle Miocene deep-water turbidite deposits located in the Gulf of Mexico (Texaco Gulf of Mexico Deepwater Development, Personal Communication). They are massive to laminated, fine-grained unconsolidated sandstones with low clay and cement content. The three sands have an average effective porosity range of 27-30% and an average permeability range of 800-1200 md. Starting at a depth of approximately 9500 feet SSTVD (Sub-sea and true vertical depth), the X-1 sand has a true vertical thickness range of 25-95 feet.

The deeper X-2 and X-3 sands each have a thickness range of 20-30 feet. Updip to the northeast, the X-1 sands are more massive and well developed, while they become thinner and more membered downdip towards the southwest. The X-2 is thinner than the X-1 but generally more massive and regular in thickness. Where encountered, the X-3 sand is membered and similar in gross interval thickness to the X-2 sand above it. Formation Micro-Induction (FMI) dipmeter log data indicate depositional movement of the turbidites from a west-northwest direction. A depositional model built from interpretation of the 3-D seismic data suggests that the turbidites filled a minibasin and backstepped into incised canyons of the Cretaceous carbonate shelf. In the seismic section in Figure 2, the sands are viewed as low impedance (peak over trough, or blue over red) events that onlap the strong high impedance reflection from the Cretaceous carbonate. Note that in this figure, as well as in the rest of the paper, arbitrary depth and time shifts have been applied to the data for display purposes.

Water-flood well plan

Acoustic impedance (AI) has been used extensively for reservoir mapping in this area as it was found to be a reliable facies indicator. The AI attribute is obtained by inversion of seismic data (e.g., Francis, 1997). Figure 3 shows AI maps of the X-1 and X-2 sands. The hotter, orange and red, areas correspond to stronger acoustic impedance. Strong AI values were found to correlate with blocky sands lacking lamination. The maps also show simplified well plans for the water-flood production of each reservoir. The red well is located in the gas cap, the green wells are oil producers, and the blue wells are water injectors. Based on analysis of pressure data and fluid flow simulations,

if normal depletion drive recovery is assumed, then one could only expect to produce 50% of the oil that could be produced using a water flood. Therefore, the development plan calls for injection of 36,000 barrels of water per day to repressurize the reservoir and to sweep the oil from the injectors updip toward the producers. This secondary recovery process should dramatically increase production throughout the life of the field.

METHODS

Initially, the field well logs were corrected from measured depth to true vertical depth and minor edits were made using the *GMAplus* software. Next, the log data were modeled using known in-situ pore-fluid properties along with end-member cases in which each of the reservoirs were assumed to be full of water, oil, or gas. Additionally, fluid properties were modeled that were extracted from a snapshot of a fluid-flow simulation model after a time lapse of five years. Petrophysical modeling was performed with the *PetroTools* software. The detailed petrophysical modeling workflow is documented in Appendix A. A summary of the modeling parameters is listed in Table 1. Default constants (*PetroTools*, 1996), were used for bulk and shear modulus (Table 1) with the exception of the densities that were increased to 2.67 g/cm3 for both quartz and clay to account for the high iron content in the illite/smectite-bearing clays. All three reservoirs are undersaturated with 31° API oil gravity, 0.68 gas specific gravity, and a brine salinity of 90,000 ppm. The gas/oil ratio (GOR) is 669 scf/BBL in the X-1 reservoir, and 900 scf/BBL in the X-2 and X-3 reservoirs.

Field logs were compared to computed logs derived from effective media models (e.g., Berryman, 1995) to verify consistency in the log data. Where available, the field

shear sonic logs were deemed noisy and not very reliable. A number of different methods were tested to predict shear sonic logs in Wells A and D where the full sonic logging suite existed. The Greenberg-Castagna (1992) shear prediction model had the closest agreement with the measured shear. Discrepancies were attributed to inaccuracies and noise in the measured shear sonic logs. For consistency purposes, all shear sonic logs were discarded and replaced by Greenberg-Castagna predictions.

The fluid substitution cases were computed using the standard Biot-Gassmann technique (Biot, 1956; Gassmann, 1951; Mavko et. al., 1998). The purpose of fluid substitution (Figure 4) is to compute new P- and S-wave velocities and density as in-situ pore fluid is replaced by a new fluid. To test the validity of this method, a fluid substitution was performed on a reservoir that is nearly full of oil in-situ that is replaced with 100% oil saturation. There was an expected agreement in velocities and density between the field and predicted logs. Several other methods were tested, e.g., effective media models, but their predictions were not as accurate.

AVO behavior was analyzed using two methods. The first method (Fuqua and O'Neill, 2000) involves computing reflectivity based on an idealized half-space model. Within a depth range of interest, clay volume, porosity, and fluid saturation curves drive the decomposition of the well logs into lithologic classes. These classes are important during fluid substitution, as, e.g., clay will not be affected by a fluid change due to its low permeability. The (fluid) substituted formations are then averaged to a half-space model for which reflectivity is computed using the full Zoeppritz equations (Zoeppritz 1919, Aki and Richards, 1980).

The second method is simpler but computationally intensive. Synthetic seismic offset gathers were generated using a fully elastic layerstack method (Aki and Richards, 1980), which includes all multiples and conversions. The source wavelet was a 20 Hz Ricker with a –90° phase shift which was used to best resemble the field wavelet. It is understood that there are resolution limitations using this wavelet, however, the objective was to simulate the real seismic data as closely as possible. A spherical divergence correction was applied, and normal move-out removed. Next, the seismic amplitudes in each of the synthetic gathers were picked and plotted versus offset. Amplitudes were picked by selecting the maximum negative amplitude that represents the sand in each offset trace within a gather.

Both methods yield a list of amplitudes versus offsets. They may be overlaid within the same figure in order to interpret the results. As comparisons are made, it should also be noted that the amplitudes from the synthetic seismic gathers include variations due to wavelet effects, which do not affect the idealized models.

Investigations pertinent to modeling

Density-Porosity Relationships.-The *PetroTools* program requires density (ρ) and porosity (ϕ) be consistent according to the following empirical relationship: $\rho_{rock} = (1-\phi)\rho_{solid} + \phi\rho_{fluid}$. An inconsistency in this relationship was observed in Well A, when porosity was computed from density. While the relationship held for all of the shales, the average porosity for the X-1 sand was only 28%, too low compared to 32% from the measured porosity curve. Core data also confirmed that an average porosity of 32% was expected. It was concluded that the density log was affected by invasion of drilling fluids

into the formation, which does not represent the true geologic response necessary to build the dry rock frame for the models. To correct the problem, a new density curve was computed from porosity using the empirical relationship mentioned above, and this computed log was used for the entire modeling exercise on Well A.

A more severe inconsistency due to invasion of drilling fluid was observed in Well B. This well is located in the gas cap of the X-1 sand. The oil-based drilling fluids displaced the gas in the reservoir near the wellbore yielding a density log which resembles that of the oil-filled case. Therefore, the field density log does not represent the true fluid properties, and was also replaced by a new density log computed from the gas-filled fluid substitution model to define the in-situ case.

Tuning and overburden effects.-The results of the AVO analyses of all reservoirs investigated in this paper revealed that all of the synthetic gathers were severely affected by the overburden and thin-layer tuning. This conclusion led to an investigation into the effects of amplitude corrections for tuning and overburden effects on the AVO responses. Three corrections were applied: calibration, overburden correction, and zero-offset (static) tuning correction. The first correction attempts to remove transmission losses due to overburden effects as well as the original source strength. A method proposed by Chiburis (1987) normalizes the target amplitudes with regard to a shallower reference reflector. Unfortunately, there is no reference reflector readily available in this data set. Therefore, the method was modified by computing synthetic gathers for an overburden-over-reservoir-half-space model. Amplitudes were picked for these synthetic gathers and

fitted with a polynomial curve, which is simply a higher order Shuey (1985) approximation:

$$d(t,x) = A + B\sin^2\theta(t,x) + C\sin^4\theta(t,x), \qquad (5)$$

where t is two-way travel time, $\theta(t,x)$ is angle of incidence as a function of offset x, and A, B, and C are weighting coefficients. The ratio between the polynomial and the ideal Zoeppritz half-space at normal incidence was used to calibrate all synthetic gathers for source strength, transmission and attenuation losses, and residual divergence.

Offset-dependent overburden effects were removed by scaling the polynomial to the Zoeppritz idealization. Since the overburden is not affected by the fluid substitution, the same offset dependent scaling function can be applied to all cases concerning the same well.

The last correction relates to tuning: Widess (1973) and Bakke and Ursin (1998) showed that thin layers strongly affect amplitudes. Hence, a constant factor was estimated to correct tuning at zero offset. Bakke and Ursin (1998) also suggested an offset-dependent tuning correction, which we neglected as it yielded inconsistent results; it under-corrected the water-sand cases, and over-corrected the hydrocarbon-sand cases. A *Mathematica* program was written to perform the corrections described above and plot the results.

Pressure effects.-In order to study the impact of pressure effects on the AVO response, an additional fluid substitution was performed by changing fluid saturations to the 5-year case while neglecting the change in pressure. Compaction effects were not taken into account in any of the models. Any deviation between the 5-year AVO

response with the change in pressure from that without the change in pressure would suggest a pressure effect on the AVO response. This test was performed on the X-1 sand in Well A and the X-2/3 sand in Well D.

RESULTS OF PETROPHYSICAL MODELS AND AVO ANALYSES

Well A

Well A is located in the updip area where the X-1 sand is well developed, massive and 96 ft thick. Table 2 shows the reservoir properties that were used for modeling. In-situ, the reservoir has an oil saturation of 78%. Three end-member cases were modeled for this location using 100% saturations of water, oil, or gas, while keeping all other reservoir conditions constant. The fluid-flow simulation model showed that in five years, water will have swept this location, with 38% of the oil remaining in place. Also, the pore-pressure of the reservoir will have dropped below bubble point, causing a small amount of free gas to come out of solution. Since the GOR depends on pore-pressure, it is decreased accordingly.

Figure 5 illustrates the log responses for the in-situ and fluid substitution cases. The reservoir is highly saturated with oil, as validated by the close agreement of the in-situ (black) and 100% oil (green) substitution responses. Relative to in-situ responses, P-wave velocity, density, and Poisson's ratio are decreased in the 100% gas (red) substitution, but increased in the 100% wet (blue) and 5-year (pink) substitutions. S-wave velocity, however, remains unchanged since the shear modulus is unaffected by the fluid.

The synthetic seismic gather computed from the in-situ case is shown in Figure 6. The X-1 sand layer is represented by the low impedance event between 3.34 sec (top) and 3.36 sec (base). The P and S-wave sonics and density log are also displayed. Using the *GMAplus* Well Editor program, this view was created to show the difference in resolution between the seismic data and the well logs, and to display the seismic response of the overburden.

The same synthetic gather was calibrated to the real seismic survey as shown in Figure 7. Unfortunately, no CDP data is available, but three angle stacks were built from field data: near (0-15°), mid (15-25°), and far (25-35°) (e.g., Nada and Shrallow, 1994). In Figure 7, the near and far angle stacks are shown to the right of the synthetic gather. The amplitude trends of the angle stacks correlate qualitatively with the AVO behaviors computed for the in-situ case, as both show an increase in amplitude with offset of the trough representing the X-1 sand, which supports the validity of the numerical models. The CDP traces in the angle stacks denoted by the symbol 'x' were used for correlation with the synthetic traces.

Results of the idealized analytical Zoeppritz AVO are shown in Figures 8a and 8b. The curves in Figure 8a are reflectivity versus angle of incidence. The same curves are shown in Figure 8b but mapped to the offset domain. The offset range of 0-15,000 ft corresponds to 0-35° incident angles. The same color scheme used in the well log view has been applied to the reflectivity plots: black for in-situ, red for gas, green for oil, blue for water, and pink for five years. The wet and 5-year cases have normal incidence reflectivity, or intercept, near –0.05 that is weaker than for the hydrocarbon cases, where

in-situ/oil are –0.11 and gas is –0.15. The AVO curve is nearly flat for the wet case, meaning that its gradient is nearly zero. The 5-year curve has a slightly negative gradient (Class III) (Rutherford and Williams, 1989, and Castagna et al, 1998) because the oil in the reservoir has not been fully swept in five years. The in-situ, oil, and gas cases all have stronger negative gradients (Class III) relative to the 5-year case.

Figure 9a shows the AVO responses of all of the fluid cases computed from the idealized models (Figure 8b) as well as from the amplitudes of the synthetic gathers. The idealized models are shown as lines, the amplitudes from the gathers are shown as dots, and the same color scheme is used for the fluid cases. Overall, normal incidence reflectivity is much larger in the synthetic gathers than in the idealized models for all fluid cases. Since the gathers contain the effect of the wavelet, this is attributed to thin-bed tuning (Widess, 1973). In fact, the thickness of the X-1 sand (96 ft.) is just below a quarter wavelength of the source wavelet (112.5 ft.), therefore, it is near maximum tuning where amplitudes are doubled by constructive interference. The tuning effects magnify the gradients as well, as observed by a much stronger positive gradient in the water and 5-year cases, and a much stronger negative gradient in the gas case, which is consistent with earlier findings by Lin and Phair (1993).

The results from our attempt to remove the overburden and tuning effects are shown in Figure 9b. The overburden correction uses the polynomial fit (5) to the amplitudes computed from the overburden/half-space model (Figure 10) and the analytical Zoeppritz model. The zero-offset value of the polynomial was used to calibrate the amplitudes of the overburden-over-half-space synthetic gather to the in-situ

idealized curve which is used as a reference. The full polynomial was used to correct the amplitudes for offset-dependent overburden effects. A factor of two tuning correction is also applied because the amplitudes in Figure 9a are two times larger than the idealized amplitudes. Similar offset-dependent scale functions were obtained for other wells and sands.

The tuning correction resolved the normal incidence tuning well, with the exception of the gas case, which is still under-corrected. The overburden correction flattened the gradients somewhat. Nevertheless, there remain differences between the corrected amplitudes and the idealized curves which may be explained by errors in the overburden correction, wavelet effects, amplitude picks, and offset-dependent tuning effects. Also, at far offsets greater than 12,000 ft., the synthetic data appear to be contaminated by multiples and conversions.

Due to the large residuals even after overburden and tuning corrections, it is concluded that these corrections are impractical, especially because we cannot easily apply them to a real 3-D seismic survey as they are model-based. Similarly, we cannot account for them when inverting seismic data for AVO attributes. We are unable to reduce the AVO data to a half-space equivalent, hence we cannot apply Landrø's (2001) empirical relationship between changes in AVO and reservoir parameters. But, provided acquisition and processing are consistent, for this dataset it is assumed that tuning and overburden will have the same effect on each of the repeat seismic surveys for either synthetic or field experiments. *Therefore, considering the specific conditions of the reservoirs in this study, we can compare repeat surveys to determine relative changes in*

attributes, and it is not necessary to apply these corrections in the time-lapse experiment. In many cases it appears that overburden and tuning corrections will not be necessary to observe meaningful time-lapse amplitude differences. However, in the general case, the subsurface conditions may require consideration of these corrections. If the velocity variation due to fluid change produces a significant travel time difference to the base of the reservoir, then the tuning effect may become problematic. In this study, the travel time differences are less than 2 msec. and thus tuning differences can be ignored. An extreme case is in shallow steam-flood applications, where the velocity change is so significant that it is used for the time-lapse information instead of the amplitude change (Jenkins et al, 1997; and Waite et al, 1997). A case where the overburden correction could be important is a produced reservoir above the reservoir being considered for time-lapse. In this case, the overburden correction could be ignored only if the monitor survey was acquired after the shallower reservoir was produced.

Since amplitude corrections were considered unnecessary for the reservoirs in this study, AVO attributes were computed directly using the amplitudes from the calibrated gathers in Figure 9a, and are reported in Table 3. As we are particularly interested in the effect of the water-flood, only the in-situ and 5-year cases are given. The in-situ intercept (A_0) is –0.205, the 5-year (A_5) intercept is –0.139, the intercept ratio (A_5/A_0) is 0.678, and the relative change in intercept ($\Delta A=(A_5-A_0)/A_0$) is 0.322. The in-situ gradient (B_0) is –0.002, the 5-year gradient (B_5) is 0.248, the gradient ratio (B_5/B_0) is 117.19, and the relative change in gradient ($\Delta B=(B_5-B_0)/B_0$) is 118.19. Conservatively assuming a 20% relative-change detectability threshold, clearly the changes in both attributes due to

water-flood at this location should be observable in a seismic survey. Due to its magnitude, relative change of gradient (ΔB) appears to be more diagnostic of the water-flood than relative change of intercept (ΔA).

Well-D

Well D is located in the downdip area where the X-2 and X-3 sands are fairly membered. The X-2 and X-3 reservoirs share the same reservoir properties (Table 2), and will be commingled during production. The 27 ft. thick X-2 and the 54 ft. thick X-3 are considered to be a single 108 ft. thick interval as the seismic data cannot resolve them independently. The reservoirs are nearly full of oil in-situ. In 5 years, the fluid saturations will not change, except for a small amount of free gas released as the pore pressure will drop below bubble point.

Figure 11 illustrates the log responses for the X-2/3 sand, using the color scheme as before. The membered nature of the sands makes interpretation difficult, but again, there is close agreement between the in-situ and oil substitution. As expected, relative to the in-situ responses, P-wave velocity, density, and Poisson's ratio decrease for the gas substitution, but increase for the water substitution. There is also some agreement between the in-situ and 5-year case, since the fluid saturations do not change.

The synthetic seismic gather computed from the in-situ case is displayed in Figure 12. The X-2/3 sand layer is represented by the low impedance event between 3.54 sec (top) and 3.565 sec (base). Although not shown here, the gather was also compared to the near and far angle stacks of the field seismic survey, which exhibited a similar amplitude behavior.

The AVO responses of all of the fluid cases computed from the idealized models as well as from the amplitudes of the synthetic gathers are shown in Figure 13a. The idealized models are shown as lines, while the amplitudes from the gathers are shown as dots. The same color scheme is used for the fluid cases. Compared to the results for the X-1 sand in Well A, the idealized Zoeppritz curve for the wet case has a positive gradient, but the intercept is larger (–0.09) because each individual sand has a different impedance effect. The hydrocarbon intercepts are also larger: in-situ and oil cases are –0.16, the 5-year case is –0.14, and the gas case is –0.19. The gradients of all the hydrocarbon cases are different for the X-2/3 sand in this well; they are all slightly positive.

Tuning is observed again on the amplitudes of the calibrated synthetic gathers (dots), but the amplitudes are lower than those in their respective idealized curves even though the thickness of the interval is similar to that of the X-1 Sand in Well A. A possible explanation is tuning or destructive interference between the reflections from thin sand members, which diminishes amplitudes compared to the idealized half-space model.

In Figure 13b, a factor 0.9 tuning correction and an offset dependent overburden correction based on an overburden-half-space model have been applied to the synthetic gathers. Again, the static tuning correction works well, but the gradients from the synthetics do not match the ones from the idealized models. The synthetics may be affected by errors in the overburden correction, wavelet effects, amplitude picks, and

offset-dependent tuning effects. We infer that, at large offsets, the amplitudes are also contaminated by multiples and converted arrivals.

Neglecting amplitude corrections, relative time-lapse AVO attributes were computed from the calibrated gathers in Figure 13a, and are reported for the in-situ and 5-year cases in Table 3. Unlike Well A, here we are interested in the behavior of the attributes in an area that will not yet be swept by the water-flood after 5-years of production. The in-situ intercept (A_0) is –0.123, the 5-year (A_5) intercept is –0.112, the intercept ratio (A_5/A_0) is 0.914, and the relative change in intercept ($\Delta A=(A_5-A_0)/A_0$) is 0.086. The in-situ gradient (B_0) is –0.273, the 5-year gradient (B_5) is -0.150, the gradient ratio (B_5/B_0) is 0.548, and the relative change in gradient ($\Delta B=(B_5-B_0)/B_0$) is 0.452. Conservatively assuming a detection threshold of 20%, the relative change in intercept will not be detectable. The change in relative gradient, however, is much larger, and should be detectable.

PRESSURE EFFECTS

Despite the maintenance of reservoir pressure by water injection, there will be a certain decrease in pore pressure in each reservoir after five years of production (Table 2). Velocity is dependent on pressure in each petrophysical model; therefore, we examined how changes in pore pressure affect the change in AVO, with the assumption there are no compaction effects. Figures 14a and 14b show idealized Zoeppritz curves for the X-1 sand from Well A and the X-2/3 sand from Well D, respectively. Each well represents a different mechanism. In Well A, the pressure change accompanies a dramatic change in fluid saturation in 5-years due to the water-flood, while in Well D,

only the pressure changes, but the saturations do not because the injected water has not yet reached the well (Table 2). As a test, a new set of well logs was computed for the 5-year parameters while keeping pressure constant at in-situ levels. In each figure, the original 5-year AVO response with a change in pressure is shown in pink, and the new 5-year AVO response modeled without a change in pressure is shown in light blue. Clearly, there is a pressure effect on the AVO response. The deviation is slightly greater in Well A than in Well D because the pore pressure decrease in the X-1 sand (1,223 psi) is greater than in the X-2/3 sand (950 psi). However, the deviation between the blue and pink curves is very small as compared to the deviations between the AVO responses of the fluid cases. Therefore, the pressure effect is considered secondary to the fluid saturation effects on the AVO response, which is consistent with earlier findings by Gardner (1981).

CONCLUSIONS

Several methods for AVO analysis have been published in recent years. This work is a case study that illustrates the importance for understanding both the geological and geophysical characteristics of the true earth model before attempting to simulate it.

Despite our attempts to remove the tuning and overburden effects from the synthetic gathers, some problems were inherent such as residual errors and contributions of multiples and converted waves at the far offsets (>10,000 ft). These effects would also be present in the real seismic surveys, and it is difficult to remove them or to account for them consistently using a model-based approach. However, in a time-lapse experiment, one is not interested in absolute attributes, but rather their changes between surveys.

Provided there is good repeatability, and tuning, overburden, and lithology affects the data in the same manner in every survey, differences between surveys are detectable despite incomplete corrections. By assumption, the overburden does not change while the surveys and processing are performed as consistently as possible. Hence, one may attribute differences to changing reservoir conditions, i.e., fluid saturations. Especially for hydrocarbon to brine substitutions, we observed significant differences in our uncorrected models, suggesting that the water may be delineated from hydrocarbons in spite of complications from tuning and the overburden. Therefore, we prefer to work with calibrated data only, instead of trying to remove overburden and tuning effects. We will follow the same strategy when dealing with the field data.

In the two examples that were discussed in this study, values for A and B were reported, however, these values will vary away from the wells as fluid saturations, and to a lesser degree, pore pressures change. Intercept, which is dependent on impedance, will also vary as sand thickness and quality changes from blocky to laminated. The results of the fluid substitutions showed that the water-filled reservoir has significantly different AVO attributes than the hydrocarbon-filled reservoir. The water-filled reservoir has more positive gradients and lesser intercepts than hydrocarbon reservoirs.

Based on our findings from AVO analysis, the relative change in intercept (ΔA) and relative change in gradient (ΔB), both could be used to monitor the water-flood. Assuming a 20% relative detection threshold, the relative changes in both intercept and gradient due to the water flood are seismically detectable, enabling the use of time-lapse AVO for monitoring production. The relative change in gradient is very large in an area

that has been swept by the water-flood. But even in an area that has not been swept and the pressure dropped below bubble point, the relative change is still above our conservative threshold. It may be possible to use this difference to gain further insight into the production, but for the purpose of monitoring change, we believe that relative changes in AVO gradient are very diagnostic for time-lapse monitoring of production from this field.

REFERENCES

Aki, K., and Richards, P.G., 1980, Quantitative seismology: Theory and methods, Freeman and Co., San Francisco.

Bakke, N.E., and Ursin, B., 1998, Thin-bed AVO effects, Geophysical Prospecting, Vol. 46, p. 571-587.

Batzle, M., and Wang, Z., 1992, Seismic properties of pore fluids, Geophysics, Vol. 57, p. 1396-1408.

Berryman, J.G., 1995, Mixture Theories for Rock Properties, in *A Handbook of Physical Constants*, T.J., Ahrens, ed. American Geophysical Union, Washington D.C.

Biondi, B., Mavko, G., Mukerji, T., Rickett, J., Lumley, D., Deutsch, C., Gundeso, R. and Thiele, M., 1998, Reservoir monitoring: A multidisciplinary feasibility study, The Leading Edge, 17, no. 10, 1404-1414.

Biot, M.A., 1956, Theory of propagation of elastic waves in a fluid saturated porous solid, I. Low-frequency range and II. Higher-frequency range, J. Acoust. Soc. Am., Vol. 28, p. 168-191.

Castagna, J. P., 1993, AVO analysis-tutorial and review, *in* Offset Dependent Reflectivity-Theory and Practice of AVO Analysis, J. P. Castagna and M. Backus, eds., Investigations in Geophysics, No. 8, SEG, Tulsa, Oklahoma, p.3-36.

Castagna, J. P., Han, D. and Batzle, M. L., 1995, Issues in rock physics and implications for DHI interpretation, The Leading Edge, 14, no. 08, 883-885.

Castagna, J. P., Swan, H. W. and Foster, D. J., 1998, Framework for AVO gradient and intercept interpretation, Geophysics, Vol. 63, No. 03, p. 948-956.

Chiburis, E.F., 1987, Studies of amplitude versus offset in Saudi Arabia, 57th SEG Meeting, Expanded Abstracts, p. 614-616.

Ebrom, D., Krail, P., Ridyard, D. and Scott, L., 1998, 4-C/4-D at Teal South, The Leading Edge, 17, no. 10, 1450-1453.

Fuqua, A., and O'Neill, B., 2000, Optimizing petrophysical modeling and seismic amplitude analysis using a consistent highly integrated workflow, EAGE Meeting, Petrophysics meets Geophysics, Paris, Expanded Abstracts.

Francis, A., 1997, Acoustic impedance inversion pitfalls and some fuzzy analysis, The Leading Edge, Vol. 16, No. 3, p. 275-278.

Gardner, G. H. F., Wyllie, M. R. J., and Droschak, D. M., 1981, Effects of pressure and fluid saturation on the attenuation of elastic waves in sands, *in* Seismic wave attenuation, Johnston, D. H., ed., Soc. of Expl. Geophys., p. 42-51.

Gassmann, F., 1951, Über die Elastizität poröser Medien, Vier. der Natur. Gesellschaft in Zürich, Vol. 96, p.1-23.

Greenberg, M.L., and Castagna, J.P., 1992, Shear-wave velocity estimation in porous rocks: Theoretical formulation, preliminary verification and applications, Geophysical Prospecting, Vol. 40, p. 195-209.

Hill, R., 1952, The elastic behavior of crystalline aggregate, Proc. Phys. Soc. London, A65, p. 349-354.

Hilterman, F., 1989, Is AVO the seismic signature of rock properties?, 59th SEG Meeting, Expanded Abstracts, p. 559.

Jenkins, S. D., Waite, M. W., Bee, M. F., 1997, Time-lapse monitoring of the Duri steamflood: A pilot and case study, The Leading Edge, Vol. 16, No. 10, p. 1267-1273.

Landrø, M., 2001, Discrimination between pressure and fluid saturation changes from time-lapse seismic data, Geophysics, Vol. 66, No. 3, p. 836-844.

Lin, L., and Phair, R., 1993, AVO Tuning, 63rd SEG Meeting, Expanded Abstracts, p. 727-730.

Mavko, G., Mukerji, T., and Dvorkin, J., 1998, The rock physics handbook: Tools for seismic analysis in porous media, Cambridge University Press, Cambridge, UK.

Nada, H., and Shrallow, J., 1994, Evaluating geophysical lithology determination methods in the central offshore Nile Delta, Egypt, 64th SEG Meeting, Expanded Abstracts, p. 1112-1113.

Ostrander, W.J., 1984, Plane-wave reflection coefficients for gas sands at nonnormal angles of incidence, Geophysics, Vol. 49, No. 10, p. 1637-1648.

PetroTools, Version 2.5, Rock Solid Images, San Jose, CA, 1996.

Reuss, A., 1929, Berechnung der Fliessgrenze von Mischkristallen, Zeitschrift für Angewandte Mathematik und Mechanik, Vol. 9, p. 49-58

Rutherford, S.R., and Williams, R.H., 1989, Amplitude-versus-offset variations in gas sands, Geophysics, Vol. 54, No. 6, p. 680-688.

Shuey, R.T., 1985, A simplification of the Zoeppritz equations, Geophysics, Vol. 50, No. 4, p. 609-614.

Smith and Gidlow, 1987, Weighted stacking for rock property estimation and detection of gas, Geophysical Prospecting, Vol. 35, p. 993-1014.

Verm, R., and Hilterman, F., 1995, Lithology color-coded seismic sections: The calibration of AVO crossplotting to rock properties, TheLeading Edge, Vol. 14, No. 8, p. 847-853.

Voigt, W., 1928, Lehrbuch der Kristallphysik, Teubner, Leipzig.

Waite, M. W., Sigit, R., 1997, Seismic monitoring of the Duri steamflood: Application to reservoir management, The Leading Edge, Vol. 16, No. 10, p. 1275-1278.

Wang, Z., 1997, Feasibility of time-lapse seismic reservoir monitoring: The physical basis, Leading Edge, Vol. 16, No. 9, p. 1327-1329.

Widess, M. B., 1973, How thin is a thin bed, Geophysics, Vol. 38, No. 6, p. 1176-1254.

Zoeppritz, K., 1919, Erdbebenwellen VIIIB, On the reflection and propagation of seismic waves, Gottinger Nachrichten, I, p. 66-84

TABLES

Table 1: Petrophysical modeling parameters (*PetroTools*, 1996).

Mineral	Density Constant (g/cm^3)	Bulk Modulus (GPa)	Shear Modulus (GPa)
Clay	2.67	20.861	6.8548
Quartz	2.67	36.6	45.0

Table 2: Reservoir properties used for petrophysical modeling.

	Case	Water Saturation (%)	Oil Saturation (%)	Gas Saturation (%)	GOR	Avg. Effective Pressure (psi)	Avg. Pore Pressure (psi)
Well A, X-1	T_0 In-situ	22	78	0	669	4665.7	4845.0
	T_0 Wet	100	0	0	669	4665.7	4845.0
	T_0 Oil	0	100	0	669	4665.7	4845.0
	T_0 Gas	0	0	100	669	4665.7	4845.0
	T_{5yrs}	61	38	1	580	6615.8	3622.0
Well D, X-2/3	T_0 In-situ	23	77	0	900	4905.5	5260.0
	T_0 Wet	100	0	0	900	4905.5	5260.0
	T_0 Oil	0	100	0	900	4905.5	5260.0
	T_0 Gas	0	0	100	900	4905.5	5260.0
	T_{5yrs}	25	74	1	760	5351.4	4310.0

Table 3: Intercept (A) and Gradient (B) Information.

	A_0	A_5	A_0/A_5	$\Delta A = (A_0/A_5)/A_0$	B_0	B_5	B_0/B_5	$\Delta B = (B_0/B_5)/B_0$
Well A, X-1	-0.205	-0.139	0.678	0.322	-0.002	0.248	117.19	118.19
Well D, X-2/3	-0.123	-0.112	0.914	0.086	-0.273	-0.150	0.548	0.452

FIGURES

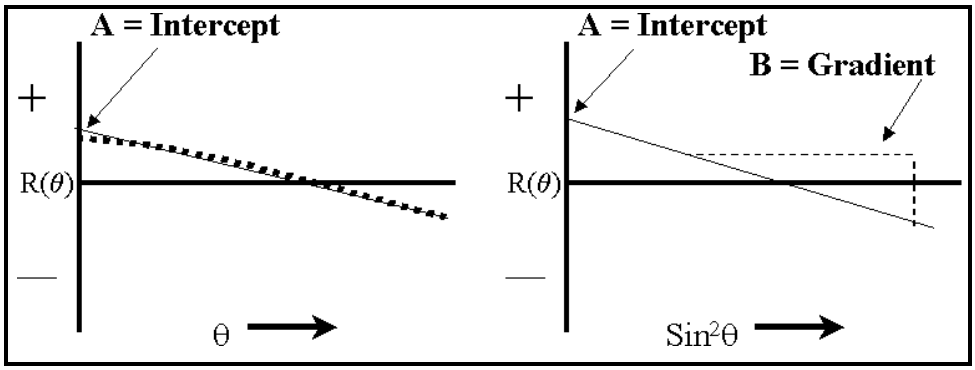

Fig. 1. Amplitude-derived seismic attributes.

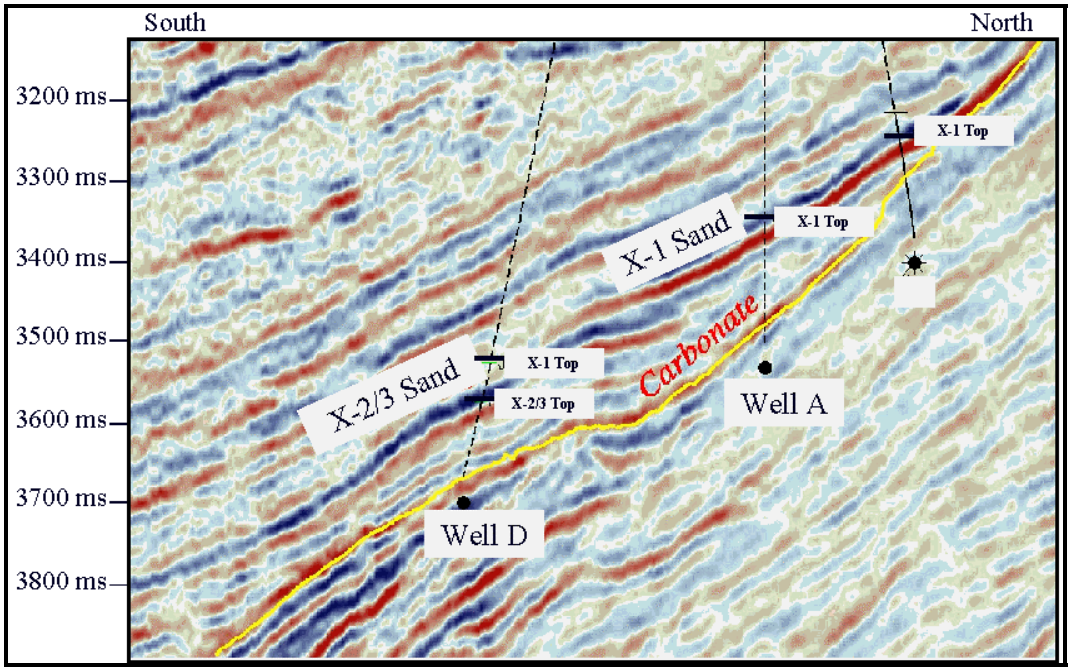

Fig. 2. Seismic dip line. X-1, 2, and 3 Sands and Wells A, B, and D shown.

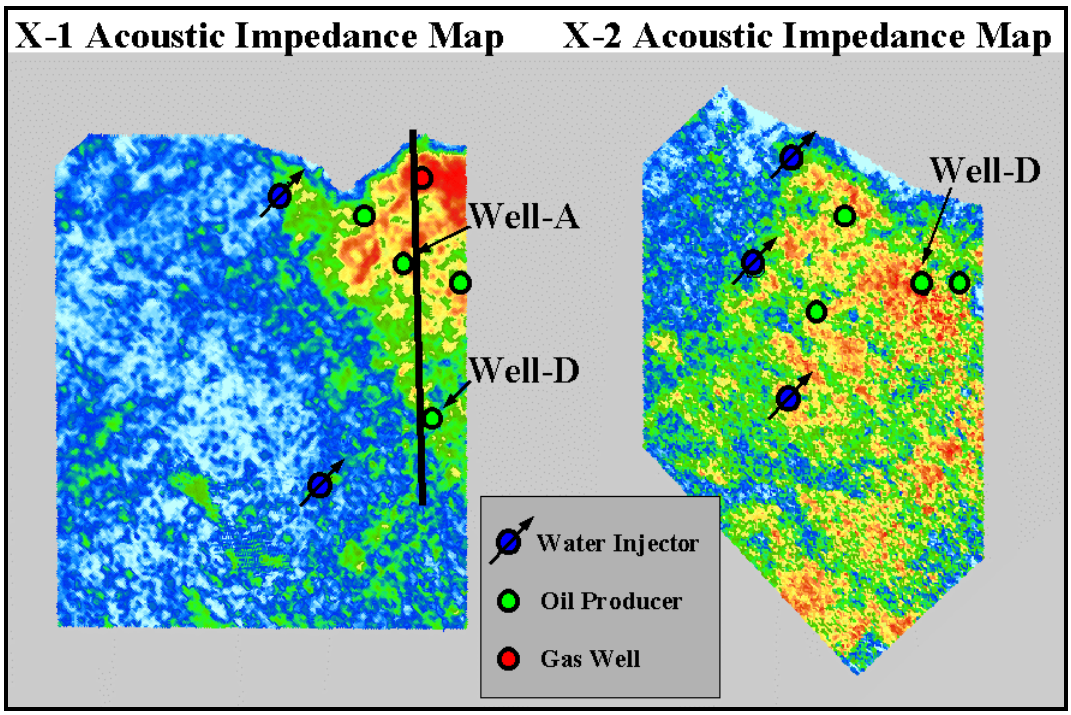

Fig. 3. Acoustic impedance maps of the X-1 and X-2 sands. The red color corresponds to strong negative impedance. Water-flood well plan shown along with wells used for modeling in this study. Orientation of the seismic line in Fig. 1 indicated by black line.

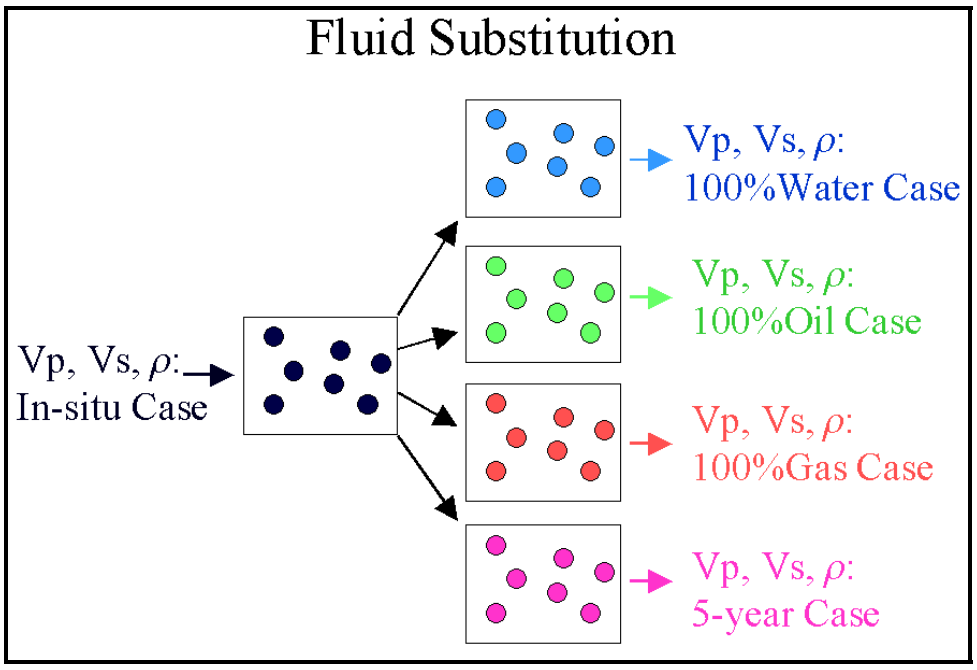

Fig. 4. Fluid substitution diagram.

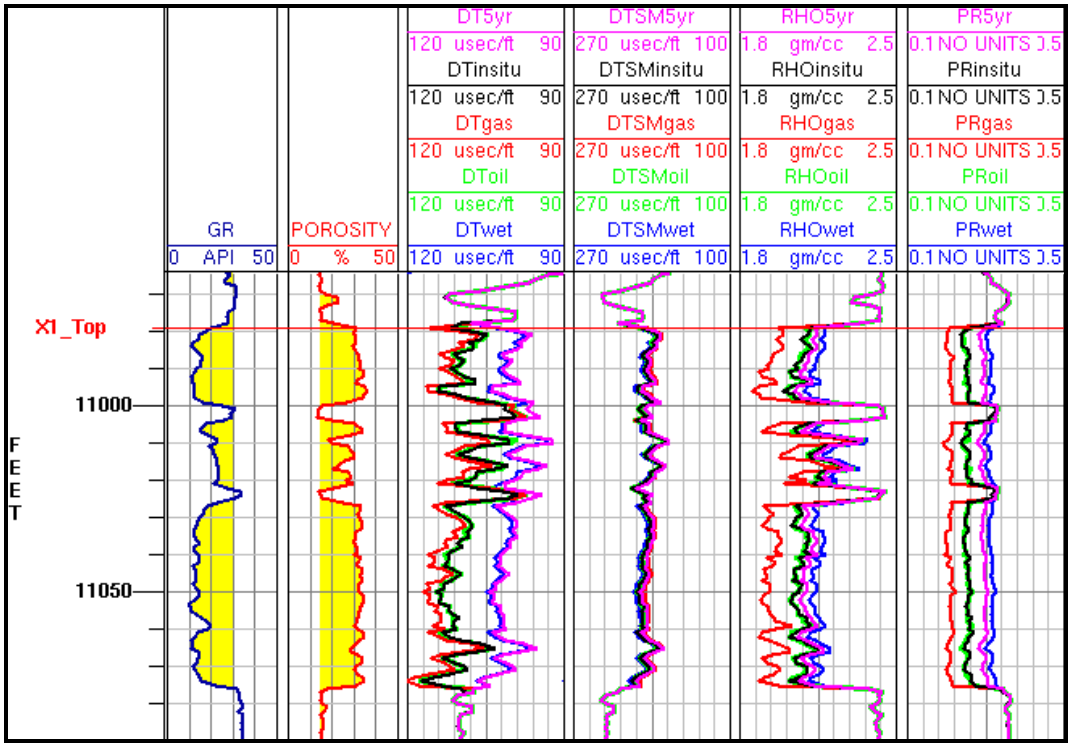

Fig. 5. Well Log view and results of petrophysical models of the X-1 sand in Well A. Log responses shown: Gamma Ray, Porosity, DT-compressional sonic, DTSM-shear sonic, RHO-bulk density, and PR-Poisson's Ratio. In-situ shown in black, oil substitution in green, wet in blue, gas in red, and 5-year in pink.

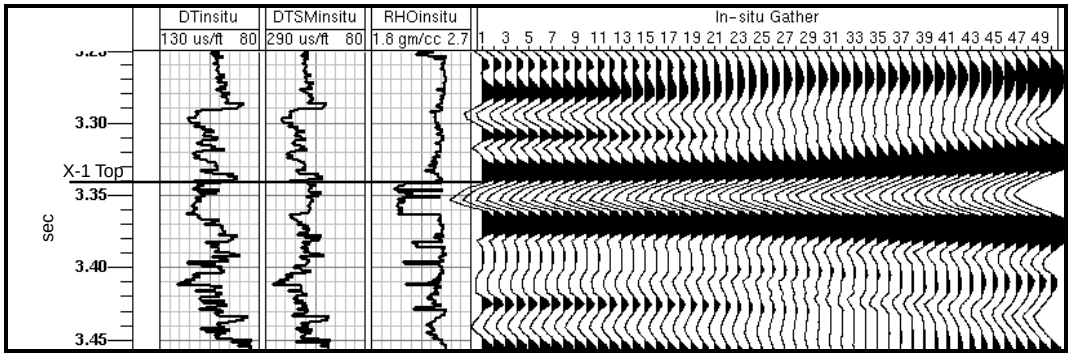

Fig. 6. Synthetic seismic offset (ft) gather computed for the in-situ case in the X-1, Well A. Also shown: DT-compressional sonic, DTSM-shear sonic, RHO-bulk density logs.

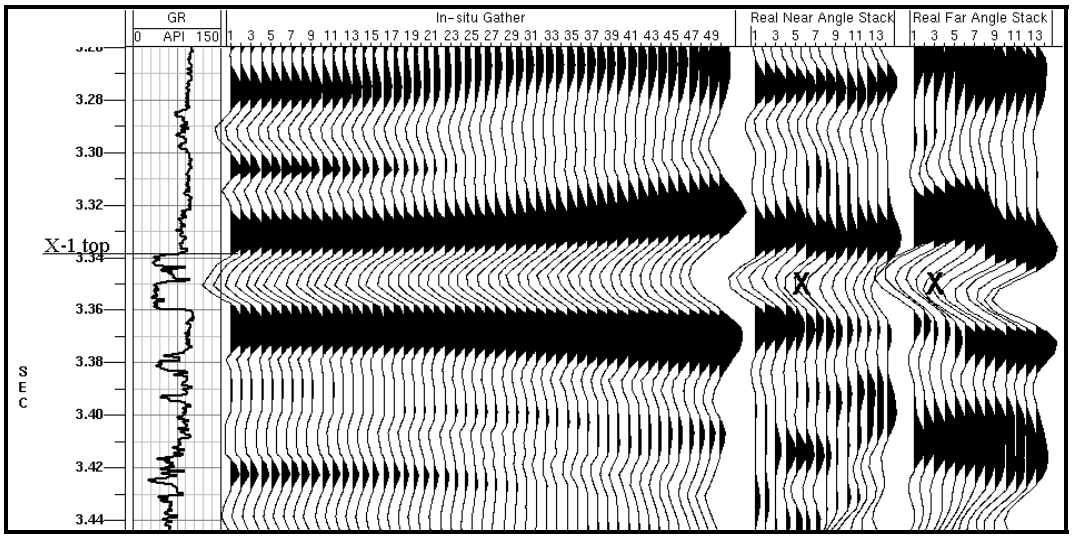

Fig. 7. Calibration of the synthetic seismic offset (ft) gather computed for the in-situ case in the X-1, Well A to real angle stacks. The 'x' symbols indicated real cdp traces used for correlation with synthetic trace. Gamma Ray log also shown.

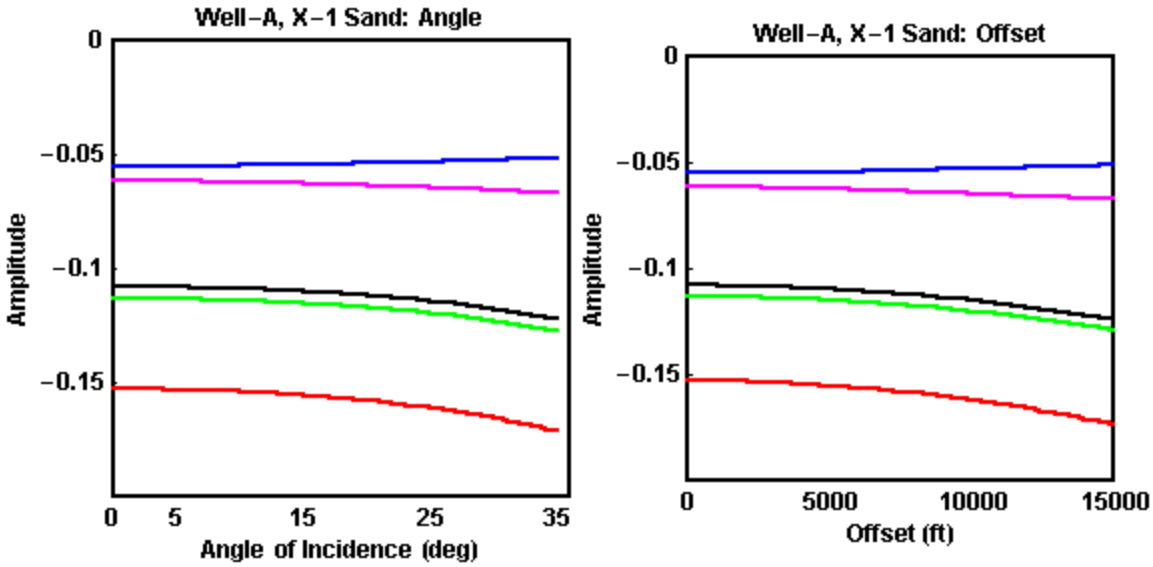

(a) (b)

Fig. 8. AVO plots for the idealized analytical Zoeppritz reflectivity for the X-1 Sand in Well A. Shown in the incident angle domain in 8a and offset domain in 8b. Black denotes the in-situ case; green denotes 100% oil substitution, red for 100% gas, blue for 100% water, and pink for 5-year case.

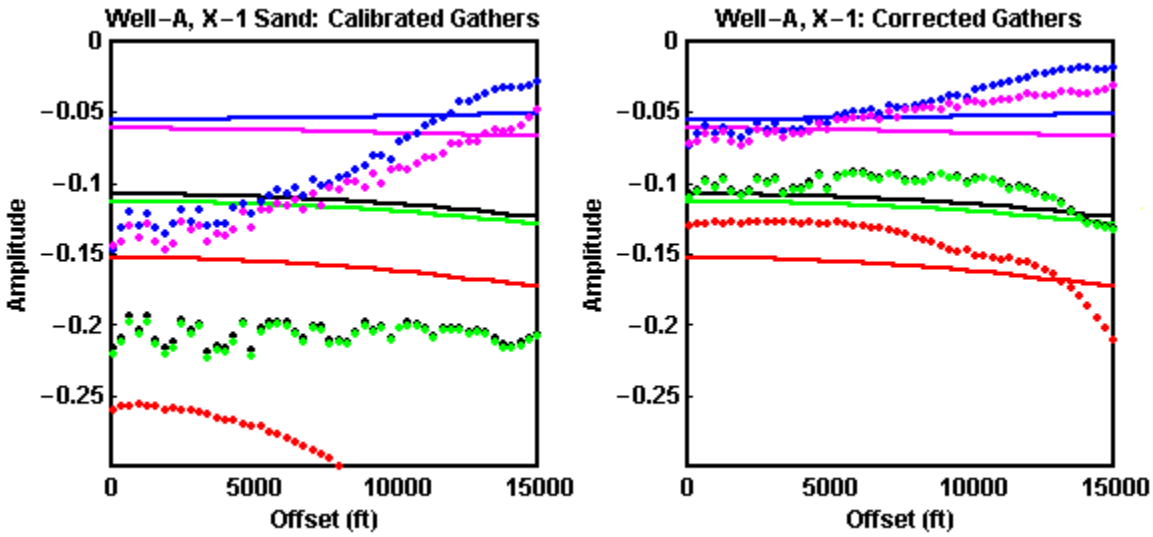

(a) (b)

Fig. 9. Tuning and overburden effects on AVO. Calibrated amplitudes (9a) and corrected amplitudes (9b) for the X-1 Sand in Well A. Idealized models shown as lines, amplitudes from synthetic gathers shown as dots. Black denotes the in-situ case; green denotes 100% oil substitution, red for 100% gas, blue for 100% water, and pink for 5-year case.

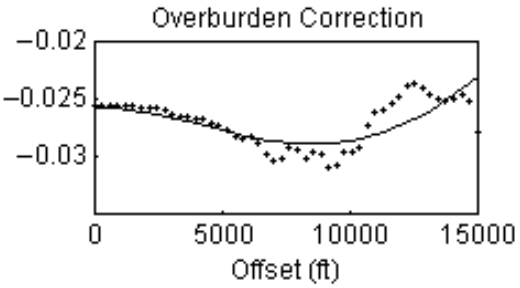

Fig. 10. Polynomial fit to the amplitude ratios computed from the overburden/half-space model versus the analytical Zoeppritz model for the X-1 Sand in Well A.

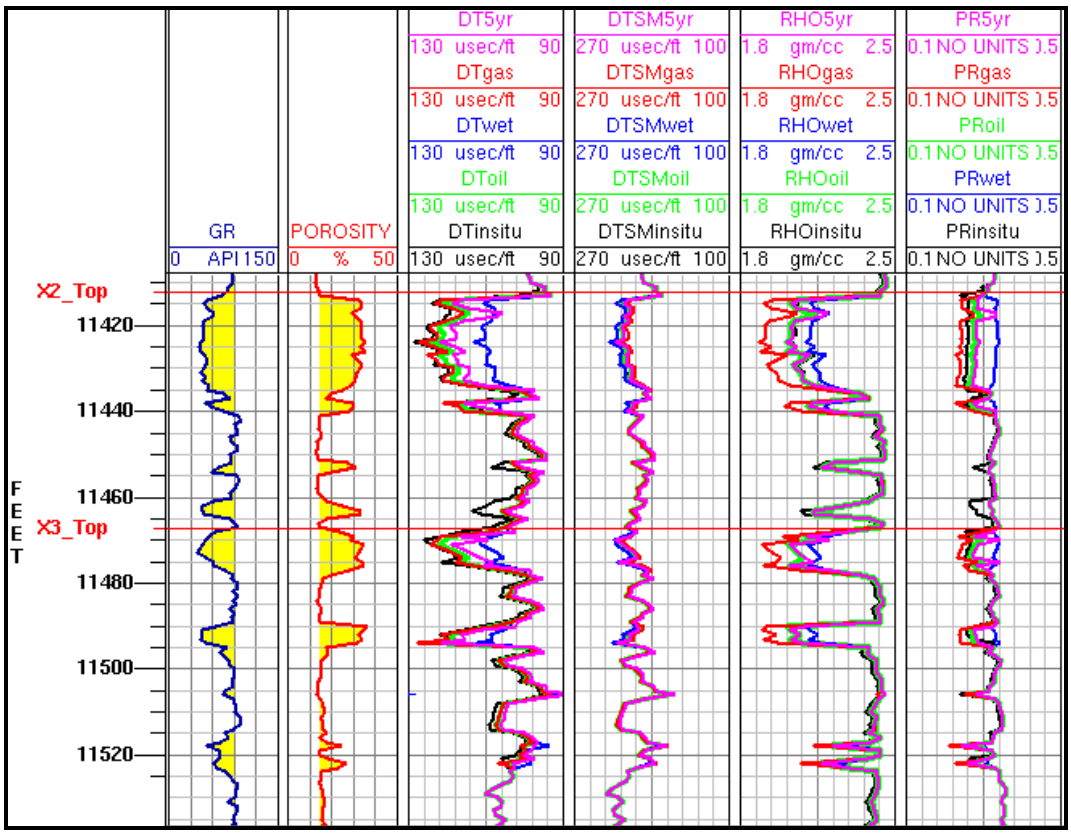

Fig. 11. Well Log view and results of petrophysical models of the X-2 and X-3 sands in Well D. Log responses shown: Gamma Ray, Porosity, DT-compressional sonic, DTSM-shear sonic, RHO-bulk density, and PR-Poisson's Ratio. In-situ shown in black, oil substitution in green, wet in blue, gas in red, and 5-year in pink.

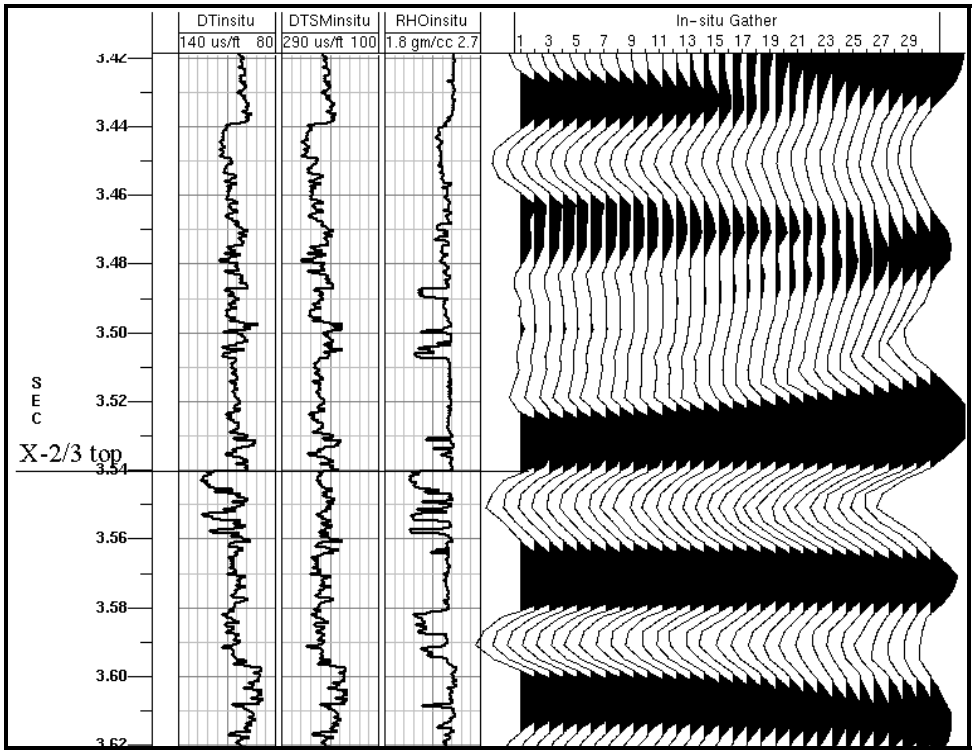

Fig. 12. Synthetic seismic offset (ft) gather computed for the in-situ case in the X-2/3, Well D. Also shown: DT-compressional sonic, DTSM-shear sonic, RHO-bulk density logs.

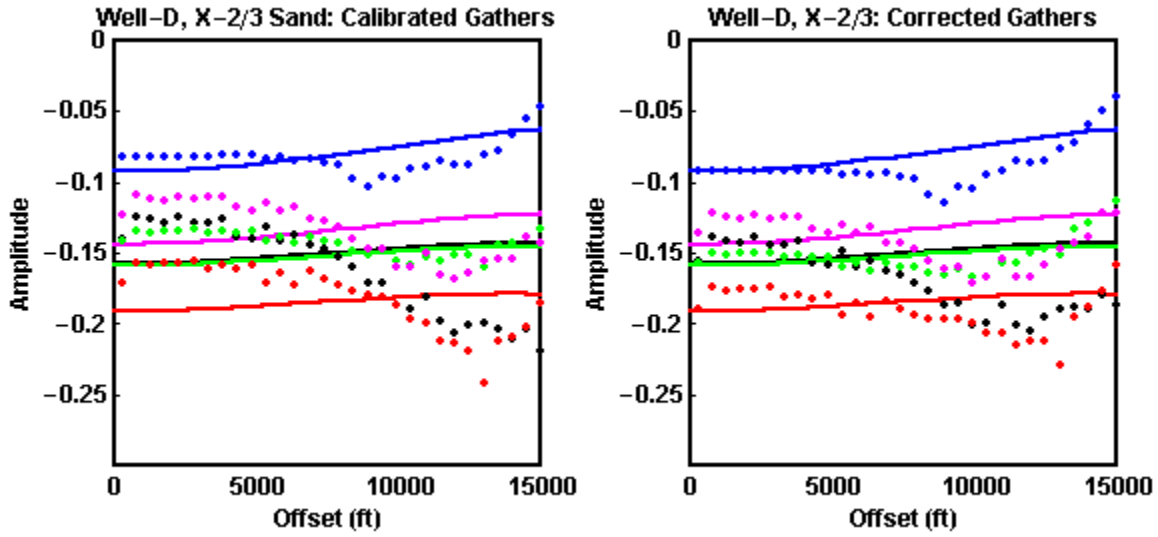

(a) (b)

Fig. 13. Tuning and overburden effects on AVO. Calibrated amplitudes (13a) and corrected amplitudes (13b) for the X-2/3 Sand in Well D. Idealized models shown as lines, amplitudes from synthetic gathers shown as dots. Black denotes the in-situ case; green denotes 100% oil substitution, red for 100% gas, blue for 100% water, and pink for 5-year case.

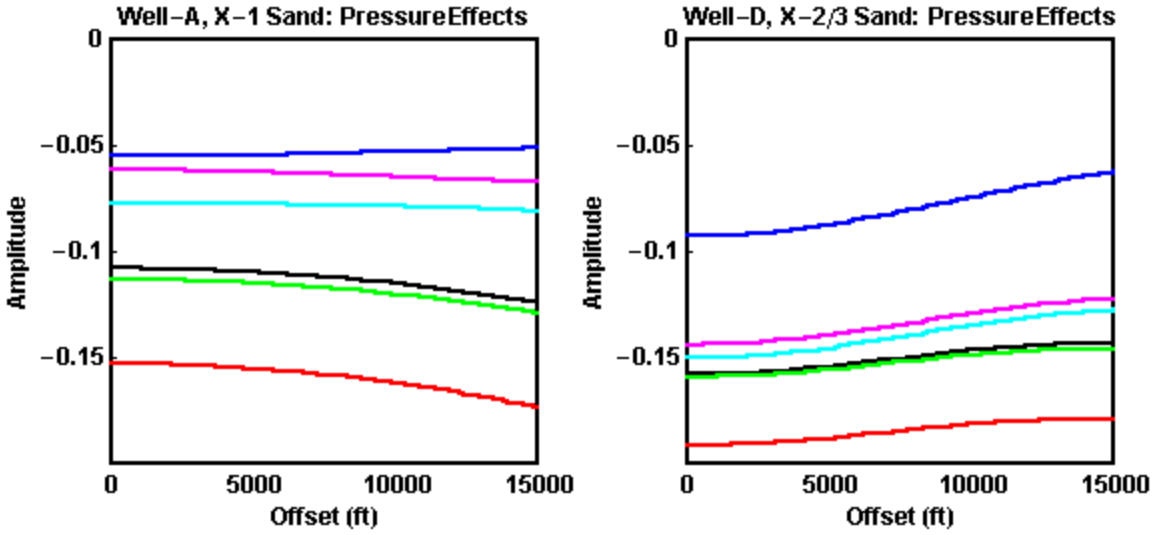

(a) (b)

Fig. 14. Pressure effects on AVO in the X-1 Sand in Well A shown in 14a; the X-2/3 Sand in Well D shown in 14b. Black denotes the in-situ case; green denotes 100% oil substitution, red for 100% gas, blue for 100% water, pink for 5-year case, and light blue for the 5-year case modeled without change in pressure.

APPENDIX A: PETROPHYSICAL MODELING WORKFLOW

The following is a generalized step by step procedure used to perform petrophysical modeling of the well log data within the program *PetroTools*:

1) Editing and import of the field (in-situ) well log data in the .las format, including: P-wave velocity (Vp), available S-wave velocity (Vs), bulk density (ρ), porosity (ϕ), water saturation (S_{brine}), clay volume (Vol_{Clay}), pore pressure (P_{pore}), and temperature (T). The logs must also be corrected to true vertical depth in advance.

2) Set Mineral and Fluid Constants: The constants found in the table below were chosen upon results from prior analysis of cuttings and core data. Default values were selected with the exception of the density constants that were slightly increased to account for high iron content in the illite/smectite-bearing clays.

Mineral	Density Constant (g/cm^3)	Bulk Modulus (GPa)	Shear Modulus (GPa)
Clay	2.67	20.861	6.8548
Quartz	2.67	36.6	45.0

3) Pressure and Temperature Gradients: Measured pore pressure and temperature logs were available. Effective pressure ($P_{effective}$) curve was computed from pore pressure (P_{pore}) according to the following:

$P_{effective}$ =[C*(Depth-Sea water depth)+D*Sea water depth] – P_{pore} ,

where the first term is the computed overburden pressure, and C and D are the gradient constants defined as:

Lithostatic, or overburden gradient (C) = 0.999974 psi/ft

Sea water pressure gradient (D) = 0.419971 psi/ft

4) Compute quartz volume from clay volume log: $Vol_{Clay} + Vol_{Quartz} = 100$

5) Compute oil and gas saturation (S) logs from the brine saturation log: $S_{oil} + S_{gas} + S_{brine} = 100$. In-situ saturations were taken from well test data; 5-year saturations from fluid-flow simulations.

6) Build a Solid, or dry rock frame:

Input: Vol_{Clay}, Vol_{Quartz}

Output: Solid (Vp, Vs, ρ, Poisson's ratio (σ), bulk modulus (κ), shear modulus (μ))

The Voigt-Reuss-Hill (M_{VRH}) average from Hill (1952) was used to estimate the moduli (M) according to the following: $M_{VRH} = (M_V + M_R) / 2$, where M_{VRH} is the arithmetic average of the Voigt (M_V) and Reuss (M_R) bounds (Voigt, 1928, and Reuss, 1929. New Vp and Vs are computed from the new moduli derived from the above equation using the following relationships:

$Vp = \sqrt{\frac{\kappa + \frac{4}{3}\mu}{\rho}}$ $Vs = \sqrt{\frac{\mu}{\rho}}$, where κ is the bulk modulus, and μ is the shear modulus.

7) Build Fluids:

Input: S_{oil}, S_{gas}, S_{brine}

Output: Brine (Vp, ρ, κ); Oil (Vp, ρ, κ); Gas (Vp, ρ, κ)

This step follows the empirical recipes of Batzle and Wang (1992) for the acoustic properties and density of fluids at various pressures and temperatures.

8) Mix the Fluids:

Input: S_{oil}, S_{brine}, S_{gas}

Output: Fluid (Vp, ρ, κ)

The "Patchy Mix" option uses the Voigt (1928) average, or upper bound, yielding the least compressible estimate of the pore fluid mixture. It is chosen because there is a significant amount of gas dissolved in the oil, and the presence of a tiny amount of gas can make the fluid less compressible. Effective modulus and density are related to volume fractions, moduli, and densities of each medium through the following equations:

$$\frac{1}{\kappa_{effective}} = \frac{S_{oil}}{\kappa_{oil}} + \frac{S_{brine}}{\kappa_{brine}} + \frac{S_{gas}}{\kappa_{gas}}$$

$$\rho_{effective} = S_{oil}\rho_{oil} + S_{brine}\rho_{brine} + S_{gas}\rho_{gas}$$

9) Shear Velocity Prediction: In-situ S-wave velocities were predicted using the Greenberg and Castagna (1992) empirical Vp-Vs relationships.

Input: Bulk Rock (Vp), ϕ, Vol_{Clay}, Vol_{Quartz}, Fluid (κ, ρ), Brine (κ, ρ)

Output: Bulk Rock (Vs, σ)

10) Fluid Substitution:

Input: Bulk Rock (Vp, Vs, ρ, κ) at Sat1

Output: Bulk Rock (Vp, Vs, ρ, κ) at Sat2

Using Biot (1956)-Gassmann (1951) low-frequency theory, the saturated rock is decomposed into a dry frame and fluid by the following:

$$\frac{\kappa_{sat}}{\kappa_{solid} - \kappa_{sat}} = \frac{\kappa_{dry}}{\kappa_{solid} - \kappa_{dry}} + \frac{\kappa_{fluid}}{\phi\left(\kappa_{solid} - \kappa_{fluid}\right)}$$

Then the rock is transformed from the saturated state to the dry state. Original fluid properties are replaced by new fluid properties, and finally the rock is transformed to the new fluid saturated state, algebraically eliminating κ_{dry}:

$$\frac{\kappa_{sat1}}{\kappa_{solid}-\kappa_{sat1}}-\frac{\kappa_{fluid1}}{\phi\left(\kappa_{solid}-\kappa_{fluid1}\right)}=\frac{\kappa_{sat2}}{\kappa_{solid}-\kappa_{sat2}}+\frac{\kappa_{fluid2}}{\phi\left(\kappa_{0}-\kappa_{fluid2}\right)}$$

Note that $\mu_{sat} = \mu_{dry}$ assuming there is no shear deformation due to the fluid substitution.

Effective κ and μ are extracted from the measured Vp and Vs, then κ is transformed to a new κ from the new fluid and is used to compute new Vp, Vs by the following relationship:

$$Vp=\sqrt{\frac{\kappa+\frac{4}{3}\mu}{\rho}} \quad Vs=\sqrt{\frac{\mu}{\rho}}$$

In addition, the new density needed in the above relationships is determined by the following relationship:

$$\rho_{effective}=\rho_{solid}\left(1-\phi\right)+\rho_{fluid}\phi$$

11) Stress Effects:

Input: Vp, Vs, $P_{effective,}$ a (30%), P_c (4351.13 psi)

Ouput: Vp, Vs, σ at new $P_{effective}$

In the 5-year case, the reservoir experiences a drop in pore pressure. This module corrects Vp and Vs for changes in net confining stress using the following formula:

$V=V_{\text{terminal}}\left(1-\left(a/1+a\right)\right)\exp\left(-P/P_c\right)$, where a is the maximum velocity change

between zero velocity and terminal velocity, and P_c is critical effective stress. Before running this module, one must compute new $P_{effective}$. First a new constant P_{pore} is assigned to the reservoir, then a new overburden pressure curve is computed, and both are used in the formula from Step 3.

To study pressure effects, the 5-year case was also modeled without the stress effects module in order to determine the impact of the change in pressure on the AVO response.

12) Export a new .las file containing the computed Vp, Vs, and ρ, as well as ϕ, S_{brine}, and Vol_{Clay} for each of the in-situ and fluid substitution cases to be used to compute Zoeppritz models and synthetic seismic gathers.

VITA

Shelley J. Ellison received her Master of Science degree in Geophysics from Virginia Tech in 2001, as well as her Bachelor of Science degree from Virginia Tech in 1998. She has accepted employment as a geophysicist in Onshore Exploration at Anadarko Petroleum Corporation in Houston, Texas upon completion of her thesis work.